THE TURBULENCE STRUCTURE OF THE STABLE ATMOSPHERIC BOUNDARY LAYER AROUND A COASTAL HEADLAND: AIRCRAFT OBSERVATIONS AND MODELLING RESULTS

IAN M. BROOKS*
Scripps Institution of Oceanography, UCSD, 9500 Gilman Drive, La Jolla, CA 92093-0209, U.S.A.

STEFAN SÖDERBERG and MICHAEL TJERNSTRÖM
Department of Meteorology, Stockholm University, Sweden

(Received in final form 28 August 2002)

Abstract. The turbulence structure of a stable marine atmospheric boundary layer in the vicinity of a coastal headland is examined using aircraft observations and numerical simulations. Measurements are drawn from a flight by the NCAR C-130 around Cape Mendocino on the coast of northern California on June 7 1996 during the Coastal Waves 96 field program. Local similarity scaling of the velocity variances is found to apply successfully within the continuously turbulent layer; the empirical scaling function is similar to that found by several previous studies. Excellent agreement is found between the modelled and observed scaling results. No significant change in scaling behaviour is observed for the region within the expansion fan that forms downstream of the Cape, suggesting that the scaling can be applied to horizontally heterogeneous conditions; however, the precise form of the function relating scaled velocities and stability is observed to change close to the surface. This result, differences between the scaling functions found here and in other studies, and the departure of these functions from the constant value predicted by the original theory, leads us to question the nature of the similarity functions observed. We hypothesize that the form of the functions is controlled by non-local contributions to the velocity variance budgets, and that differences in the non-local terms between studies explain the differences in the observed scaling functions.

Keywords: Coastline, Local similarity scaling, Stable boundary layer, Turbulence.

1. Introduction

The coastal marine atmospheric boundary layer (ABL) is an inherently heterogeneous environment. The region in which boundary-layer dynamics are directly affected by the coast extends offshore approximately one Rossby radius – up to 100 km or so (Overland, 1984). Within this region the large contrast in surface conditions between land and sea, and the constraints imposed upon the mean flow by the coastal topography, force a high degree of spatial variability resulting in a complex environment where the assumptions and simplifications that are used freely within the homogeneous ABL over the open ocean may not necessarily apply. Many coastal regions experience the frequent occurrence of stable conditions

* Current Affiliation: Institute for Atmospheric Science, School of the Environment University of Leeds, Leeds, LS2 9JT, U.K. E-mail: ibrooks@env.leeds.ac.uk

Boundary-Layer Meteorology **107:** 531–559, 2003.

resulting either from offshore flow from a warmer landmass, or the advection of a marine air mass over cool upwelling water close to the coast. The latter situation prevails along the west coasts of major continental landmasses.

Stable boundary layers are less well understood than the convective case, in part due to a lack of extensive measurements. In contrast to convective conditions, the stable ABL is not readily characterized by simple length and time scales, but is a complex function of wind speed, stratification, radiative and turbulent processes, and the time history of these factors (Nappo and Johansson, 1999). Turbulence is weak, sometimes intermittent, and often co-exists with gravity waves. Spatial heterogeneity means that measurements at a single location may not be representative of the environment as a whole. The parameterizations of surface fluxes are uncertain, particularly over the oceans where results derived from measurements over land remain largely unverified; as a consequence, numerical models tend to perform poorly for stable conditions (Nappo and Bach, 1997). Several recent studies have reported significant discrepancies between bulk estimates and directly measured surface fluxes under stable conditions (Rogers et al., 1998; Edson et al., 2000; Oost et al., 2000).

Routine meteorological measurements over coastal waters are sparse. Operational soundings are made from islands or land-based coastal stations, but suffer from contamination by land effects and are rarely representative of conditions even a few kilometres offshore (Dorman et al., 2000). A network of buoys situated 15 to 25 km offshore around the United States makes surface observations, but the buoys are widely scattered and capture only the broadest mesoscale features of coastal flow. Observations of turbulence, small-scale variability, and the vertical structure of the boundary layer offshore are limited to a handful of aircraft-based field studies (Brost et al., 1982a, b; Beardsley et al., 1987; Zemba and Friehe, 1987; Enriquez and Friehe, 1995; Brooks and Rogers, 1997). An extensive measurement program of coastal ABL structure took place off the coast of northern California and Oregon during the summer of 1996. The Coastal Waves 96 field program (CW96) was designed to address problems concerning the dynamics and mesoscale variability of the coastal boundary layer. Eleven research flights were made by the National Center for Atmospheric Research C-130 Hercules during June and early July 1996. An overview is given by Rogers et al. (1998) and results have been presented in an extensive series of publications (Burk et al., 1999; Tjernström, 1999; Ström, 1999; Dorman et al., 1999, 2000; Dorman and Winant, 2000; Edwards, 2000; Tjernström and Grisogono, 2000; Edwards et al., 2001; Haack et al., 2001; Brooks, 2001; Söderberg and Tjernström, 2001). To date the analysis of aircraft data from CW96 and associated modelling studies have focused on the mesoscale dynamics and variability. This study examines the turbulence structure and processes, and the along-wind evolution of the small-scale vertical structure of the boundary layer, utilizing both aircraft-based observations and three-dimensional (3D) numerical simulations.

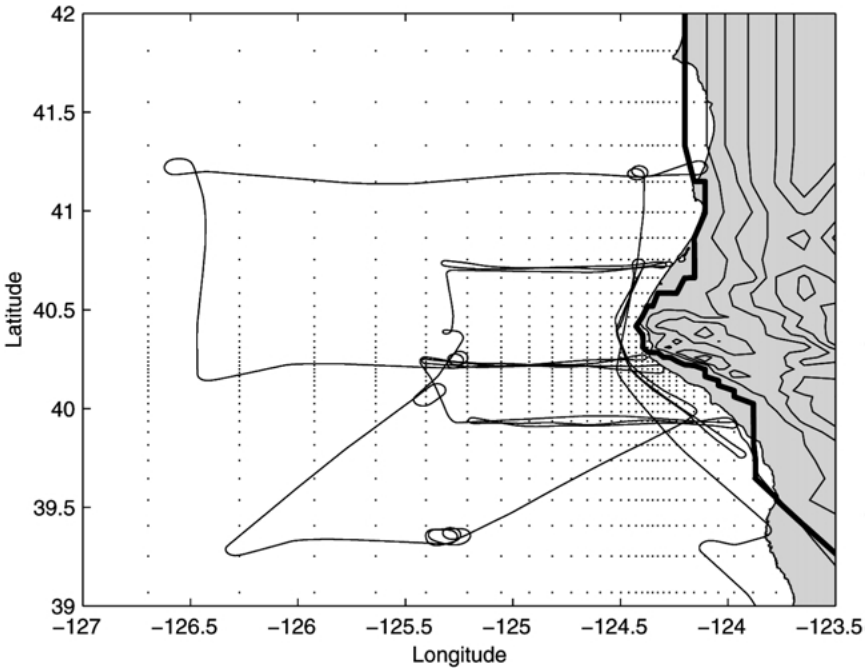

Figure 1. A map of the study area around Cape Mendocino. The aircraft flight track is shown by the solid line, The boundary-layer data were all obtained within the central region between 39.8–41 °N and 124–125.5 °W; the outer portions of the flight track were high-level runs from which dropsondes were deployed. The grid of dots shows the locations of model grid points. The coastal landmass is shaded grey, and the model terrain is contoured at 200 m intervals from sea level (heavy line).

2. Aircraft Measurements

The NCAR C-130 Hercules has an extensive suite of instrumentation for the measurement of meteorological, turbulent, radiative, and microphysical variables; details can be found in Rogers et al. (1998). All data are sampled at 25 Hz; turbulence quantities are calculated using this high-rate data, while mean quantities are derived from one-second averages.

The CW96 flight plans were designed to sample the mesoscale variability of the boundary-layer structure in the vicinity of prominent capes or headlands. Each flight consisted of a series of cross-sections through the boundary layer, made up of a series of *sawtooth* profiles extending from an altitude of 15 m to above the inversion to measure the vertical structure of the ABL, a straight and level flight-leg at an altitude of 30 m to measure near-surface fluxes, and a level flight-leg well above the inversion from which the ABL was mapped by a downward-looking lidar. Multiple cross-sections oriented perpendicular to the coast provided snapshots of ABL structure as it evolved along-wind. The flight track for June 7 is shown in Figure 1.

The primary focus on the mesoscale structure of the ABL precluded making stacks of multiple closely-spaced level flight-legs, as commonly used to measure turbulence quantities; however, the large number of profiles through the ABL (35 in total) obtained during sawtooth runs provides an alternative source of turbulence information (Mahrt, 1985; Lenschow et al., 1988; Tjernström, 1993). The time series of each variable of interest is high-pass filtered to isolate the turbulent fluctuations from the more slowly varying mean value. Filtering is performed in both the forward and reverse directions to eliminate phase shifts in the filtered time series. Profiles of instantaneous second-order moments are obtained by multiplying the filtered series together in the same manner as for direct eddy-correlation calculations. Local mean values of turbulent quantities are then found by averaging a block of the resultant series across a specified interval. For each averaging interval the wind components are rotated into a coordinate system aligned with the local mean wind. The filter pass-band and cut-off scales, and the averaging length are carefully chosen to ensure that all scales contributing to the second-order moments are included – an averaging distance of 1 km was found to be just sufficient; this corresponds to a vertical interval of approximately 50 m.

It should be noted that each such estimate of a second-order moment is only a single local realization of the true value and should not be confused with a statistically stable mean value. We have compared profile derived turbulence quantities with those from a stack of horizontal flight-legs for a later flight during the CW96 campaign. The profile-derived values lie within about one standard deviation of the mean values determined from horizontal flight legs, and gives us confidence that, while significant scatter is to be expected, the general structure of the ABL is well represented by the profile-derived turbulence quantities.

2.1. Model discussion

The model utilized here is the Department of Meteorology, Uppsala University (MIUU) mesoscale model. It is a 3D non-linear, hydrostatic primitive equations model with a modified 'Level-2.5' turbulence closure (Mellor and Yamada, 1982). The model is well documented and has been used in a variety of applications including orographic flows (Enger et al., 1993; Grisogono 1995; Enger and Grisogono, 1998) and coastal flows (Tjernström and Grisogono, 1996; Grisogono and Tjernström, 1996; Sundararajan and Tjernström, 2000). It has been used in a number of studies based on the CW96 experiment (Tjernström, 1999; Tjernström and Grisogono, 2000; and Söderberg and Tjernström, 2001) as well as more general studies of US West Coast flow (Cui et al., 1998; Söderberg and Tjernström, 2002). Detailed descriptions of the model can be found in Tjernström (1987a, b) and Enger (1990).

The terrain-influenced vertical coordinate (Pielke, 1984, pp. 118–125) expands log-linearly with height, from a resolution of 6 m at the surface to approximately 150 m at the model top (5000 m). The horizontal grid also expands (see Figure

1), in order to remove the lateral boundaries far from the area of interest while achieving maximum resolution in the model centre. Horizontal resolution at the centre of the domain is 2 km × 2 km, increasing almost linearly to about 35 km × 55 km at the lateral boundaries. The surface boundary conditions are similar to those in Tjernström and Grisogono (2000). Since the marine ABL is the focus in this study, a simple prescribed sinusoidal-type function was used for the diurnal variation of the inland surface temperature. The observed sea-surface temperature (SST) field was used, but held constant in time. Surface humidity was prescribed to produce potential evaporation at the sea surface (reduced by the salinity) and a fraction thereof (15%) over land. Skin surface values of temperature and humidity were transferred to the model grid by matching Monin–Obukhov similarity to roughness sub-layer similarity using the so called Zilitinkevich functions (e.g. Pielke, 1984).

A dynamic initialization was used in which the model is given horizontally homogeneous fields of potential temperature and humidity, and the geostrophic wind – constant in time and in the horizontal but varying with height – prescribes the background flow. The initial wind was set equal to the geostrophic wind, except in the ABL where a logarithmic profile was applied. A pre-integration period in excess of 12 hours follows during which transient gravity waves induced by the initial application of realistic surface forcing propagate out of the model domain, and the model dynamics adjust to a realistic balance between the background and local forcing. The initial and background parameter values were based on aircraft observations from 7 June 1996. The model was run and validated for conditions upstream of Cape Mendocino using the aircraft measurements (see below). An initially 1300 m deep, well-mixed ABL was capped by a 19 K and 4 g kg^{-1} inversion with stable stratification and constant (1 g kg^{-1}) humidity aloft. The geostrophic wind components (u_g, v_g) vary linearly from (-1, -9) m s^{-1} at the surface to (6, 6) m s^{-1} at 2500 m and (11, 9.5) m s^{-1} at the model top. Note that while the ABL flow is from the north, the flow aloft has a significant southerly component; this is specified in close agreement with the observed conditions. Although this case has been simulated before (Tjernström and Grisogono, 2000), the present simulation differs in several respects: the optimisation of the initialisation for the true SST and upwind of the Cape, and the use of both a new advection scheme and an improved lateral boundary condition scheme.

In an ensemble-average model the turbulence is modelled rather than simulated, and some of its characteristics are predetermined by the model closure. One cannot expect the nature of the modelled turbulence to deviate from that in the ensemble of measurements used to determine the closure constants. On the other hand, the turbulence structure of any boundary layer is controlled by the mean state of the flow. If the complexity of the turbulence is due to the complexity of the mean flow, then ensemble-average modelling may provide information on the characteristics of the turbulence; however, to the extent that turbulence in a particular atmospheric state is poorly understood on a more basic level, such simulations alone cannot be expected to shed new light on the situation. Moreover, modelled turbulence must

always be continuous and assume the presence of a well-defined turbulence spectrum. An ensemble-average turbulence model cannot, by its very nature, describe sporadic turbulence.

Another important aspect of turbulence modelling is related to the boundary conditions. In most models, including this one, the surface-layer parameters are calculated from the mean field using some form of Monin-Obukhov similarity theory. This implies an assumption of stationarity and horizontal homogeneity; we know this to often be a false assumption but hope that the effects are not critical. In a model with prognostic turbulence kinetic energy (TKE), we thus let TKE in the flow respond to the varying flow conditions with a dynamic equation that is continually forced to a boundary condition assumed to be horizontally homogeneous and in steady state. It is thus not surprising if modelled surface fluxes disagree with the observations.

The present model uses a modified version of the 'Level-2.5' closure (Mellor and Yamada, 1982). The principle behind this closure is based on a scaling argument on the complete set of second-order moment equations. Mellor and Yamada (1974) showed that the time-dependency and turbulent transport terms can be excluded in all second-order moment equations except the TKE equation (Yamada and Mellor, 1979). What remains of the higher-order equations is a prognostic equation for the TKE and steady-state analytic expressions for all the remaining second-order moments. This closure leads to unphysical negative variances when turbulence is growing (Helfand and Labraga, 1988), and the variances of the cross-stream and the vertical velocity components are equal at the surface. Both these problems are corrected for in the present scheme, the former by scaling second-order moments by the ratio of the prognostic TKE to its steady state value whenever the latter is larger, and the second by applying the so-called 'wall correction' (Andrén, 1990).

It is important here to realise the limitations – and the strengths – of this simplified modelling set-up. We use the model not as a forecast model but as a numerical laboratory, and thus wish to keep the background flow and temporal variations as simple as possible, while remaining realistic. In this manner a large degree of the forcing remains under easy control, simplifying both the analysis and sensitivity tests. Validation against the observations ensures the realistic behaviour of the model results, but it is important to note that we are more interested in examining the physical properties and processes within the flow, than in an exact correspondence between simulations and observations.

3. Synoptic Situation and Mesoscale Dynamics

The June 7 case from CW96 examined here is typical of conditions off the West Coast of the U.S.A. during the summer. Dorman et al. (2000) describe the large-scale structure of the summertime boundary layer in some detail. Synoptic con-

ditions are dominated by a region of high pressure over the north Pacific and a thermal low over North America resulting in predominantly northwesterly winds that bring air towards and along the coast. Subsidence of the air mass as it moves south leads to the formation of a strong temperature inversion at the top of the ABL, with a typical jump of 10 K or more. The inversion slopes downward from a height of about 1–2 km far offshore to a minimum of 400 m or less at the coast, where it is below the mean height of the coastal mountains, which thus act as a barrier, preventing flow inland. The mean wind exhibits a broad jet-like structure along the coast with a maximum along northern California (Nelson, 1977). Beardsley et al. (1987) found that the wind also exhibited a jet like structure in the vertical with a maximum at, or close to, the inversion and with the strongest winds within 10 km of the coast. The jet is modified through interactions of the flow with coastal topography, intensifying downwind of major headlands where the ABL thins and the flow accelerates. Winant et al. (1988) interpreted observations of such a case at Point Arena as a supercritical expansion fan. Dorman et al. (2000) found the whole coastal region to be close to critical, with extensive regions close to the coast being supercritical (the Froude number, $\mathrm{Fr} > 1$) for extended periods of time. Supercritical flow was associated with every major cape and headland; at each the flow was observed to accelerate to form an expansion fan, accompanied by a significant drop in ABL depth. Details of the spatial variability and extent of the jet have been examined in several modelling studies (Burk and Thompson, 1996; Holt, 1996; Cui et al., 1998; Edwards et al., 2001). The basic features of the flow around headlands can be reproduced by simple shallow water models (Winant et al., 1988; Samelson, 1992), but Dorman et al. (1999) noted that such models cannot explain the considerable small-scale complexity found in the aircraft observations.

The close correlation between the spatial distribution of the surface stress in the region of the expansion fan and that of the lowest SSTs has been noted previously (Rogers et al., 1998; Dorman et al., 1999; Tjernström and Grisogono, 2000; Brooks, 2001) – cold upwelling is observed along the whole West Coast, driven by Ekman pumping, but is enhanced in the lee of a headland by the strong horizontally divergent flow in the expansion fan. The lower SST results in increased stability within the lower ABL but appears to have little impact on the dynamics of the flow (Burk and Thompson, 1996; Tjernström, 1999).

4. Boundary-Layer Structure

4.1. Mean structure

Figure 2 shows maps of the ABL depth and near-surface (30 m) wind field for both the observations and the model. The observed ABL depth is estimated from the height of the temperature inversion base from aircraft profiles supplemented by lidar measurements. The observed wind field, along with other variables considered below, derives from 5-km averages along flight-legs at 30 m above the surface

linearly interpolated onto a 0.05 × 0.05 degree grid. At the offshore limit of the observations the ABL depth is a little over 600 m, falling to about 400 m close to the coast, and collapsing to just 100 m in the lee of Cape Mendocino. The model reproduces this structure well in most respects, although the large-scale gradient offshore is slightly less than that observed, and it fails to reproduce the slight increase in ABL depth close to the coast on the inside of the minimum. The observed wind field shows that the mean wind speed north of the cape is about 6 m s^{-1}, accelerating to a maximum of a little over 20 m s^{-1} downstream of the Cape. The axis of the accelerating jet around the cape is coincident with the region of maximum gradient in ABL depth. The modelled wind field shows a very similar spatial structure, but with higher wind speeds north of the Cape, about 10–11 m s^{-1}, and a maximum of 19 m s^{-1}, slightly less than that observed. The region of maximum wind speed is also slightly narrower than that observed. The model suggests that the wind-speed maximum south of the Cape has a double axis – the accelerated flow in an expansion fan, centred within the 18 m s^{-1} isotach, superposed on a broad coastal jet further offshore, indicated by the 12 m s^{-1} isotach. The observations do not extend far enough offshore to properly resolve this structure, but the upward kinks in the 10 and 12 m s^{-1} isotachs provide some support for it.

Figure 3 shows characteristic profiles of observed and modelled potential temperature and wind speed at two locations marked on Figure 2a: Upwind of the Cape at **A**, and within the expansion fan at **B**. The aircraft profiles subtend a shallow angle with the surface – the aircraft travels approximately 1 km in the horizontal for every 50 m in the vertical. In such a horizontally heterogeneous environment the aircraft profiles will be contaminated by horizontal gradients in the measured quantities. In order to provide a better comparison with the model we have plotted profiles from all the model grid points that lie within the horizontal range of each aircraft profile. At the northern point, **A**, the ABL depth is captured accurately by the model within the limits of its vertical resolution (approximately 100 m at the ABL top); the potential temperature is about 1 K too low and the wind speed within the ABL almost 2 m s^{-1} too high. The measured profile indicates that a stable internal boundary layer (IBL) has formed, approximately 300 m deep; above this the ABL appears well mixed, being the remains of the initial convective boundary layer, now isolated from surface forcing by the stable IBL. The observed wind profile is almost constant within the upper half of the ABL, indicating that little or no mixing is taking place, while the wind speed falls rapidly both within the IBL towards the surface, and upwards through the inversion. The whole upper ABL thus forms a broad wind-speed jet with the absolute maximum just below the inversion. The model does not reproduce the IBL in detail, but captures some of the structure, in particular the shape of the wind profile. Within the expansion fan the boundary layer has collapsed to a layer a little less than 100 m deep capped by an inversion several times this depth. The model captures the depth of the ABL accurately, but produces a deeper inversion with a slightly weaker gradient; the modelled temperature is about 2 K too low. The discrepancies between model and

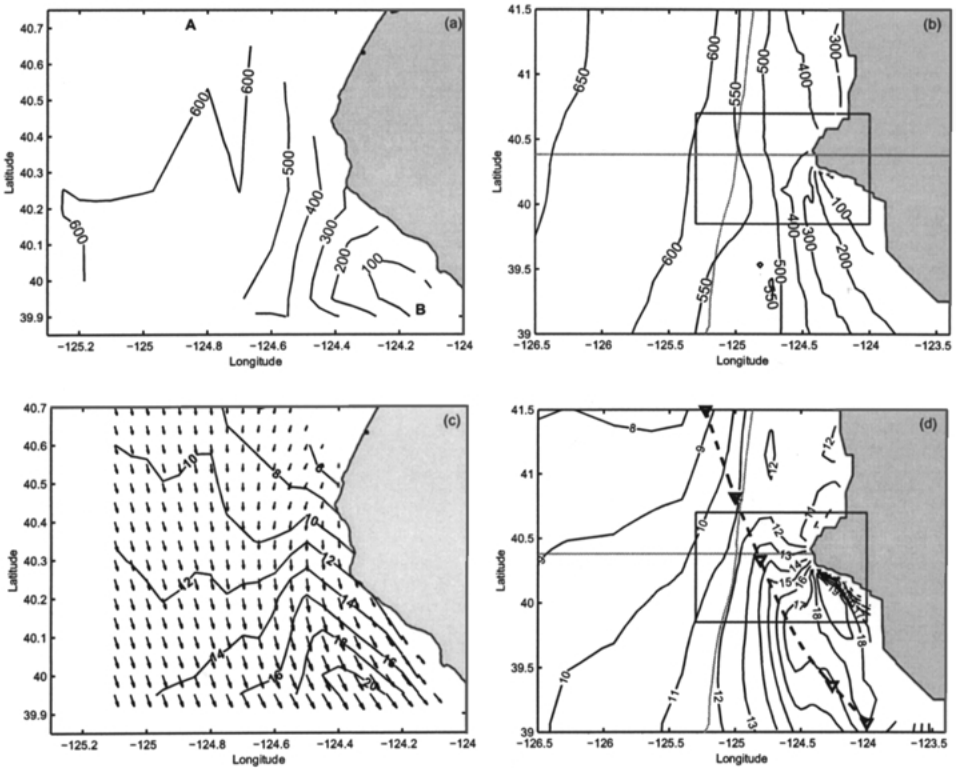

Figure 2. (a) and (b) show the observed and modelled boundary-layer depth. The points marked A and B on (a) show the locations of the aircraft profiles shown in Figure 3. (c) and (d) show the observed and modelled near-surface wind fields. The area covered by the observations is indicated on each of the maps of model results. The solid grey lines the divide the model domain approximately into quarters defining four regions with distinct dynamics: The east–west line separates the regions upwind and downwind of the cape, while the north–south line marks the Fr = 0.8 contour and separates the near-shore flow from the relatively undisturbed offshore flow. The dashed line and triangles in (d) indicate the trajectory and the divisions between distinct regions referred to in Figure 9 and Section 3c.

observations in the expansion fan may be due, at least in part, to the finite vertical resolution of the model, but also suggest that mixing within the model may be too efficient allowing the ABL temperature to fall too quickly to match the SST. This might result from the mixing-length formulation in the model. Under stable stratification a simple Blackadar-type form is used, which implicitly generates a vertically coupled turbulence field. A more local formulation might better resolve small-scale vertical structure.

4.2. Surface-layer turbulence

In model sensitivity tests the mean structure of the flow along the coast appears insensitive to the details of the surface temperature (Burk and Thompson, 1996;

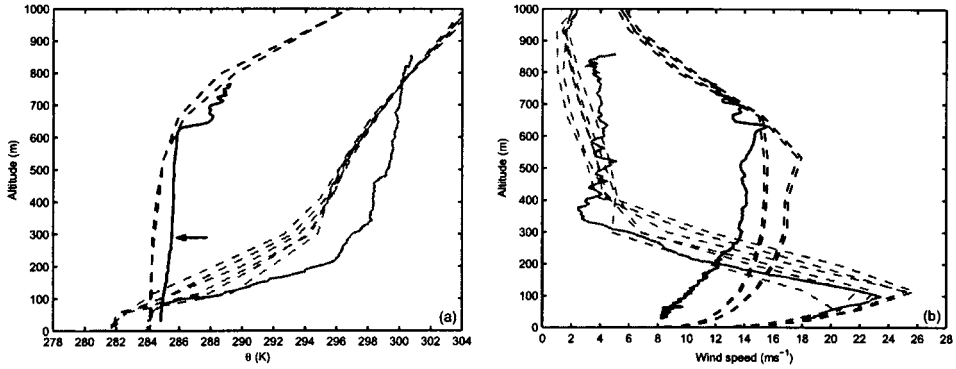

Figure 3. (a) Profiles of potential temperature at the locations A (dark line) and B (grey line) marked on Figure 2a. The dashed lines show profiles from the model for all the grid points spanned by the aircraft slant-profile. The top of the internal boundary layer is indicated by an arrow. (b) The mean wind speed for the same locations as in (a).

Tjernström, 1999; Tjernström and Grisogono, 2000); it is expected, however, that ABL turbulence characteristics in the simulation will depend upon the exact nature of the air-sea temperature difference and here the simulations are performed using the observed SST (Figure 4). There is a significant gradient in SST from west to east with cooler waters close to the coast and a localized cold pool just downwind of the Cape. The wind field shown in Figure 2 confirms the general picture discussed in Section 4 – surface-layer air moves south and towards the shore over increasingly colder waters close to the coast. We thus expect the stability of the lower ABL to increase along-wind, suppressing turbulence and vertical transport. At the same time the increasing wind speed and wind shear will act to increase turbulence generation. Figure 5 shows the two-dimensional fields of observed and modelled wind stress and virtual potential temperature (or buoyancy) flux. The observed wind stress (Figure 5a, black lines) increases dramatically from less than 0.05 N m^{-2} north of the Cape to a maximum in excess of 0.8 N m^{-2} within the expansion fan at the southern edge of the observed field. The stress distribution does not follow the wind speed exactly since it depends upon the stability as well as wind speed. Moving offshore from the axis of the jet, the ABL stability decreases and then reverses sign, becoming convective west of about 124.8° W; this provides stronger turbulent mixing and thus a higher wind stress for a given wind speed. The stress distribution is thus more uniform in an east-west direction than the wind speed, though some evidence of the wind-speed jet structure is still evident close to the coast. Also shown is a bulk wind stress (grey lines) from the TOGA-COARE bulk flux algorithm (Fairall et al., 1996). The bulk estimate of the stress is very similar in terms of the general magnitude, but differs significantly in its spatial distribution – it follows the mean wind speed very closely and tends to overestimate the local stress close to the coast, within the coastal wind-speed jet, and to underestimate the stress offshore to the southwest. There are likely to be multiple factors contributing

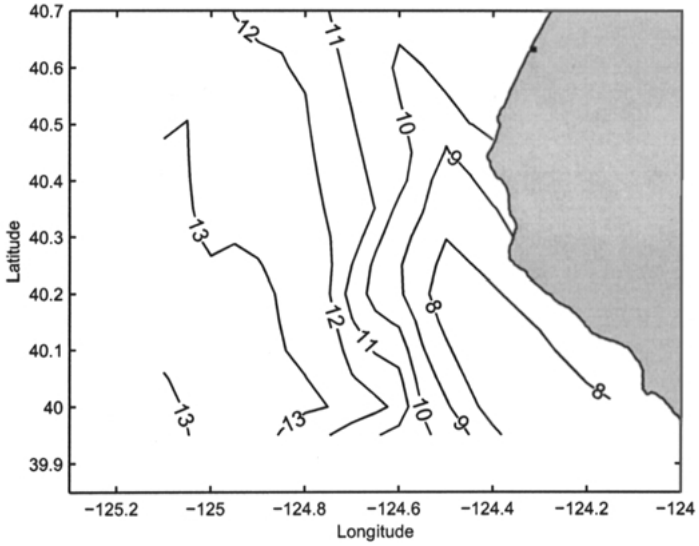

Figure 4. The observed sea-surface temperature field (°C).

to this discrepancy: The bulk formulation assumes horizontal homogeneity, clearly not the case here, thus the measured flux will include contributions from a region upstream with different conditions to those at the measurement point, while the bulk formulation uses only the local conditions. The close correlation between the bulk stress and the mean wind also suggests that the parameterization does not adequately account for changes in stability. The modelled stress (Figure 5b) has a maximum of 0.6 N m^{-2} south of the Cape, which is lower than the observed value, while the values upstream of the Cape are high by a factor of 2. This is consistent with the differences between the observed and simulated wind speed. The horizontal structure is captured successfully by the simulation. A secondary stress maximum is clearly visible west of the maximum associated with the wind speed jet and expansion fan, centred at 40° N, 124.6° W. The observations do not extend far enough south to resolve this feature, but there is some suggestion of increased stress at the far southwest of the measurement area. Figure 5c shows observed and bulk estimates of the buoyancy flux; the increasing stability over the cold pool in the lee of Cape Mendocino is obvious. The bulk parameterization significantly overestimates the magnitude of the flux, peaking in excess of -100 W m^{-2} (a negative value indicates the flux is directed downwards) while the observed value is around -60 W m^{-2}. The spatial distributions, however, agree closely. The modelled buoyancy flux (Figure 5d) overestimates the observed magnitude in a similar manner to the simple bulk estimate, but again the spatial distribution agrees well – the zero flux isoline in particular matches the observations very closely.

The curl of the wind stress is shown in Figure 6; the observed curl has a strong maximum located in the region where the stress decreases rapidly towards

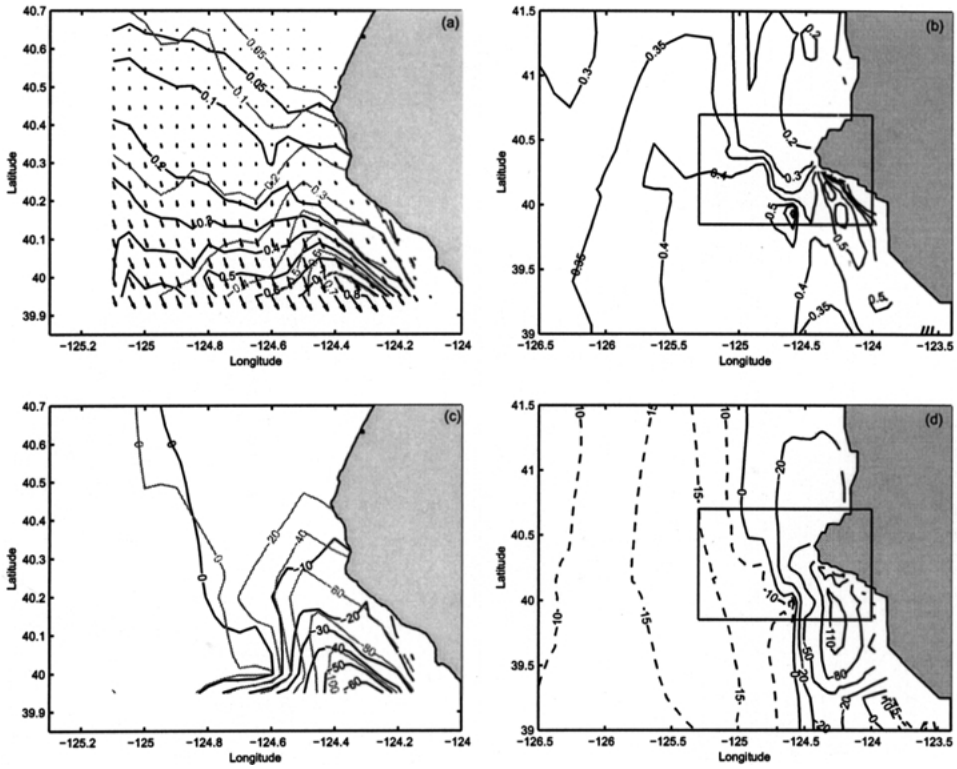

Figure 5. (a) The observed surface wind stress contours (narrow black lines) and vectors, and contours of the bulk estimates of the surface stress from the TOGA-COARE bulk flux algorithm (heavy grey lines) (N m^{-2}); (b) modelled surface wind stress (N m^{-2}); (c) and (d) show the observed (narrow black contours) and bulk (heavy grey contours), and modelled surface virtual potential temperature (buoyancy) flux (W m^{-2}); the zero flux contours are emphasised by a thicker line; positive buoyancy fluxes are contoured by dashed lines in (d). The measurement area is indicated on the model fields.

shore in the lee of the cape. The maximum observed value is approximately 5.4 $\times$ 10^{-5} m s^{-2}, far in excess of the climatological mean, but similar to values reported by Enriquez and Friehe (1995). The large positive curl results from the horizontal divergence of both the mean flow and stress, which drive divergent flow in the ocean surface layer and promote upwelling of cold water from below the thermocline. This reinforces the Ekman pumping that drives upwelling along the whole northern California coast, and results in the pool of very cold water south of the Cape. The simulated curl (Figure 6b) has a maximum a factor of 2 lower than that observed, consistent with the underestimated wind speed and stress in this region. The spatial distribution is similar to that observed, but differs in one significant respect: it features two regions of negative curl of similar magnitude to the region of positive curl. We may speculate that these features do exist but are

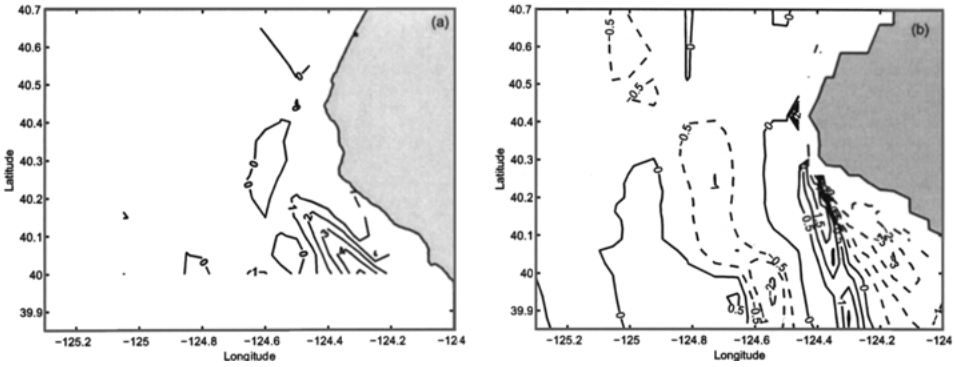

Figure 6. Maps of the observed (a) and modelled (b) wind-stress curl (10^{-5} m s^{-2}), calculated from the stress fields shown in Figure 5, both are shown for the same area.

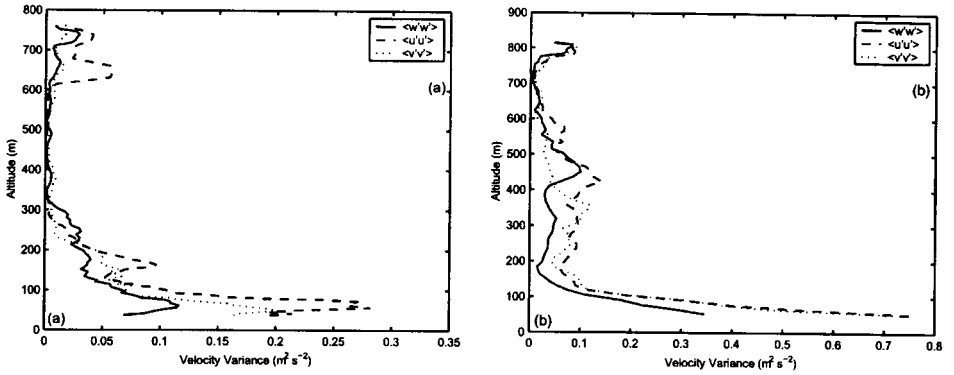

Figure 7. Aircraft profiles of the variances of the three wind components vertical (w), along-stream (u), and across-stream (v) for the locations marked A (a) and B (b) in Figure 2a.

missed by the observations due to a lack of spatial coverage, in particular the poor resolution available in the along-coast direction offshore.

4.3. Vertical turbulence structure

Figure 7 shows the variances of the three velocity components for the same profiles shown in Figure 3. Upwind of the cape turbulence is confined almost entirely within the IBL. The stable stratification is evident in the relative values of the three velocity variances: the vertical velocity variance is the weakest, with the cross- stream and along-stream variances being up to two and three times greater respectively. Within the expansion fan, turbulence is strongest within the confined boundary layer, but remains significant throughout the whole of the deep inversion layer. The cross-stream variance has increased to match the along-stream value due to a strong directional shear with altitude within the expansion fan.

Turbulence data from the model are divided into four dynamically different regions: Upstream and downstream of the cape, and near-coast and offshore (see Figure 2). The north/south division is made at the Cape, while the offshore/near-shore division is made along the $Fr = 0.8$ isoline, where Fr is the shallow-water Froude number. The modelled momentum flux for the near-shore downstream area, essentially the expansion fan, is shown in Figure 8a. Each profile is normalized by the square of the friction velocity, u_*^2, while the altitude is normalized by the ABL depth, z_i. The thick solid line is the normalized profile suggested by Lenschow et al. (1988) for stable stratification. Most of the profiles are scattered around the analytical line, with individual profiles being either more concave or convex. A striking feature is the large upward momentum flux above the ABL; this is associated with the vertical wind shear in the coastal jet, and appears only on the near-coast side of the jet (see below). Figure 8b shows normalized velocity variance profiles for the offshore upstream sector, where conditions are most homogeneous. Except for slightly elevated values in the upper 25% of the ABL, in particular in the cross-stream component, the profiles are very similar to those expected for a well-mixed near-neutral layer (Brost et al., 1982b). The surface values differ somewhat from those in Brost et al., but are well within the range suggested in the literature. The local increase below the inversion is likely related to the fact that even this far offshore the wind speed has a jet-like structure with a maximum at ABL top and decreasing aloft. In contrast Figure 8c shows the velocity variances in the expansion fan; it is clear that the ABL here is very perturbed compared to the generic homogeneous steady state on which most model closures are based. The values around the jet at ABL top are significantly higher than typical, particularly for the cross-stream component indicating a wind direction shear through the jet. There are also highly elevated values above the ABL, associated with the jet.

The substantial scatter in the curvature of the normalized momentum flux profiles in Figure 8a is a result of a complex response to many factors. Sudden changes in the surface forcing or ABL depth due to external factors such as a rapid change in SST or mesoscale variability of ABL depth will modify the overall turbulence structure at a rate determined by the existing turbulence. If the momentum flux at the surface increases rapidly, the profile is expected to become more concave; if the ABL depth is decreasing the profile should become more convex – purely from geometric considerations. An increase in the wind shear, as would be the case if the ABL depth decreases while wind speed remains constant or if the wind speed increases with a constant ABL depth, should increase mixing and thus act towards a more linear momentum flux profile. Increasing the surface momentum flux while the ABL depth decreases would also enhance mixing, forcing a more linear normalized profile. In the present case all these factors are at work; the effect of the changing balance between them is illustrated in Figure 9. It shows normalized momentum-flux profiles and wind-speed profiles plotted against normalized altitude, interpolated along the 30-m trajectory shown in Figure 2d. The trajectory is divided into four sections in which distinct differences in the balance of forcing

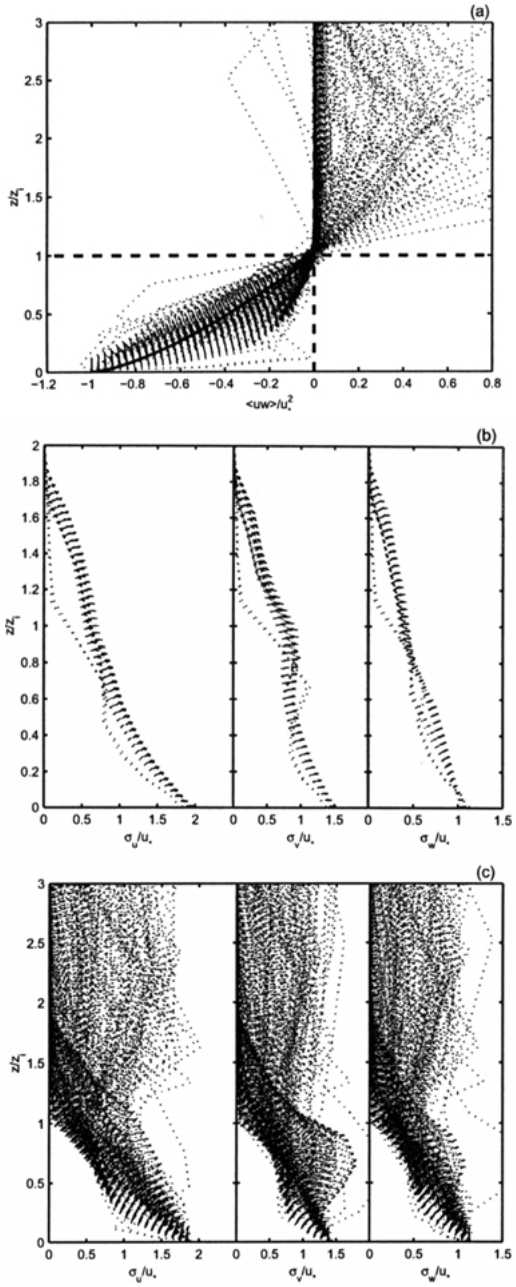

Figure 8. (a) The simulated momentum flux normalized by the square of the surface friction velocity plotted against normalized altitude for the downstream, near-shore region (essentially the expansion fan); the solid line is the profile suggested by Lenschow et al. (1988) for stable stratification. (b) Profiles of the normalized standard deviations of the three velocity components plotted against normalized altitude for the upwind, offshore region, where the flow is least perturbed by interaction with the coast. (c) as (b) but for the region within the expansion fan.

processes can be discerned. In each panel the heavy solid line denotes the first (upwind) profile, the heavy dashed line the last (downwind) profile, and the dotted lines all intervening profiles. In the first section, covering the first 95 km from north along the trajectory, the wind speed is increasing while both u_* and z_i are varying only slowly and the momentum flux profiles change only marginally. In the next section downstream, the wind speed continues to increase; here u_* increases while z_i starts decreasing and the momentum flux profile becomes more and more concave. In the third section z_i decreases rapidly and the wind speed increases the most – towards the end of this section the wind shear also has its maximum – this causes the normalized momentum flux profile to be forced back towards a more linear shape. Towards the end of the trajectory the wind speed decreases rapidly, and the normalized momentum flux profile becomes convex for a short distance before returning to linear.

Figure 10 examines more closely the modelled normalized momentum flux above the jet at $z/z_i = 1.5$. There is an area on the coastal side of the jet along the entire coast where the momentum flux is large and directed upward. The highest values are found on the inside of the jet in the expansion fan, where the upward momentum flux at this level reaches 80% of the surface value. Here it is also most clear that this feature only persists on the side of the jet with the cyclonal shear. One possible reason for this asymmetry may be that the expected secondary circulation around the jet, observed in the idealized modelling study of Söderberg and Tjernström (2001), advects warm inland air offshore on top of the jet thereby reducing the static stability to a point where the Richardson number becomes subcritical and turbulence can be sustained.

4.4. Local similarity

Local similarity theory (Nieuwstadt, 1984; Sorbjan, 1984, 1986) has proved one of the most successful frameworks within which to examine turbulence under stable conditions. It has been applied to a variety of environments including many coastal regions (Shao and Hacker, 1990; Tjernström and Smedman, 1993; Rogers et al., 1995; Bange and Roth, 1999; Brooks and Rogers, 2000). Shao and Hacker (1990) studied flow across a coastline under both stable and convective conditions and concluded that the theory could be applied to a horizontally heterogeneous environment provided that local processes were more important than external forcing. Although the local similarity theory has proved successful in many case studies, general applicability has yet to be demonstrated.

Local similarity theory can be considered as an extension of the ideas of Monin-Obukhov (MO) similarity theory above the surface layer. The local similarity scales are defined in a manner analogous to the MO scales, but depend upon local turbulence quantities at the measurement height, z, instead of surface values:

$$u_L(z) = [\overline{w'u'}^2 + \overline{w'v'}^2]^{1/4} \tag{1a}$$

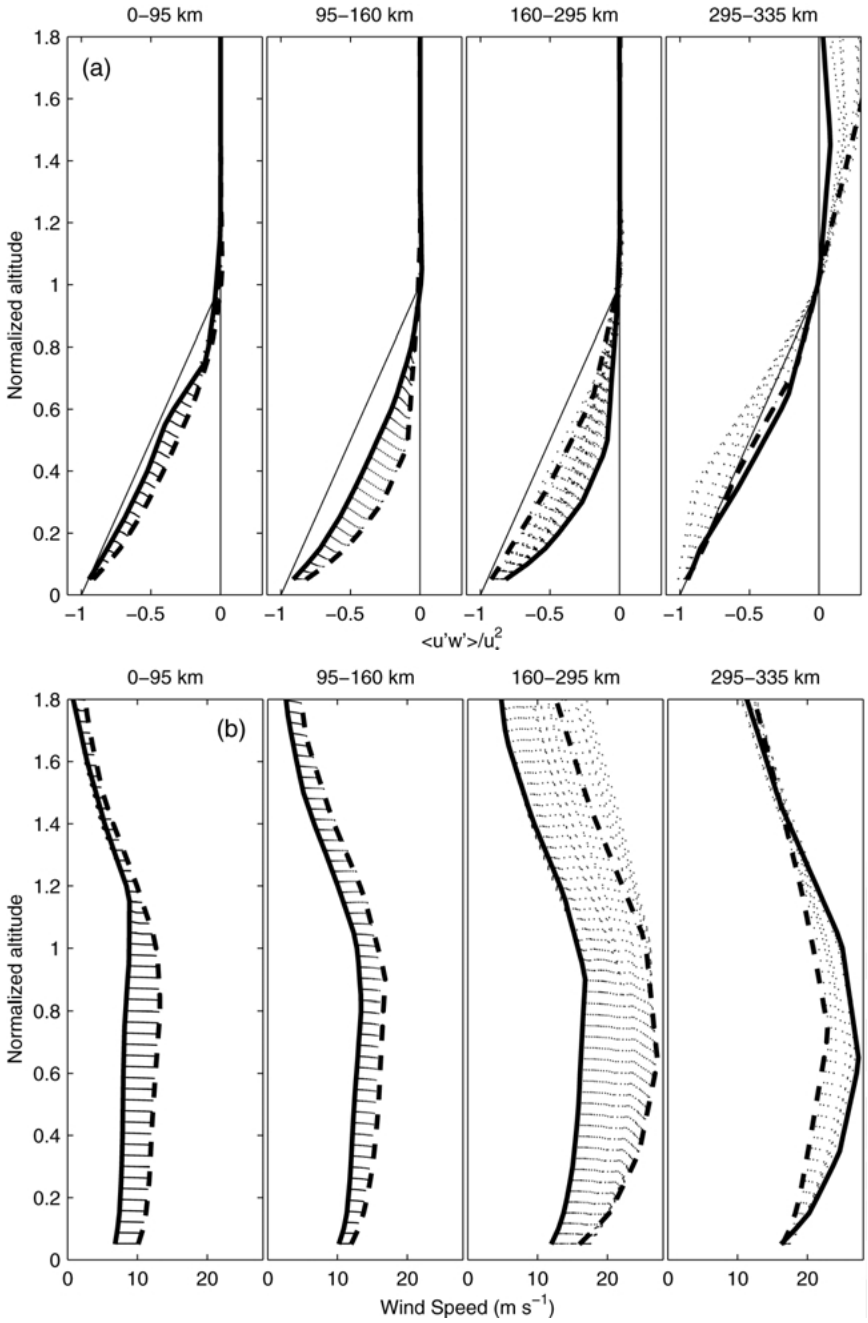

Figure 9. Normalized wind stress (a) and mean wind speed (m s^{-1}) (b) following the trajectory marked on Figure 2d. The profiles are divided into four regions along the trajectory (divisions are marked by triangles on 2d) within which a distinct change in the profile shape can be identified. The thick solid lines indicate the first (upwind) profile within each section, the thick dashed line the last (downwind) profile, and the thin dotted lines show all the profiles in between. The ideal linear stress profile expected for well mixed, neutral conditions is included as a solid line on each of the panels in (a) for reference.

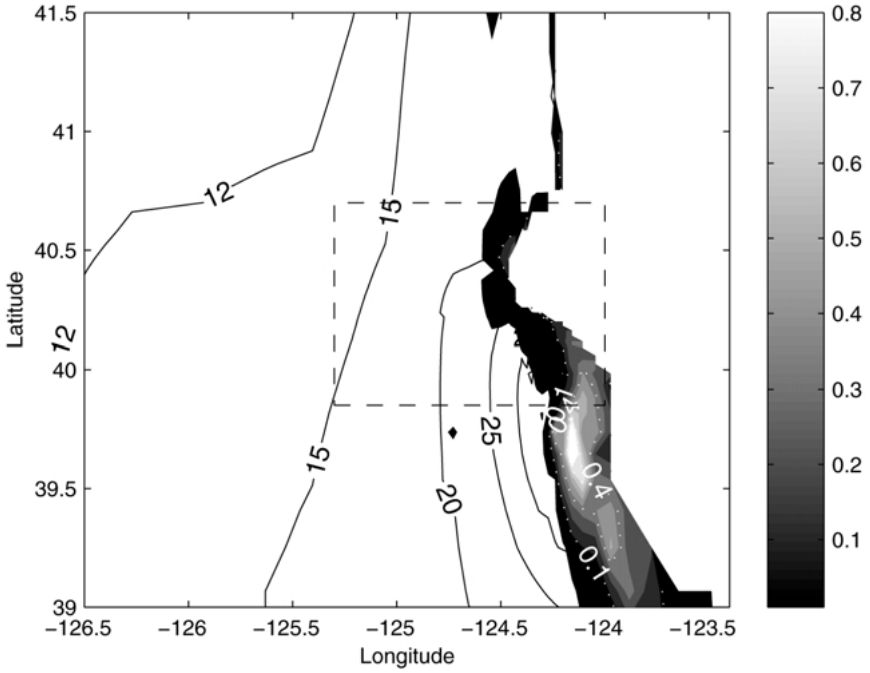

Figure 10. Mean boundary-layer wind speed (contoured) and the momentum flux at z/z_i = 1.5 (shaded for non-zero values).

$$\theta_L(z) = -\overline{w'\theta'}/u_L \tag{1b}$$

$$L_L(z) = -u_L^3/[\kappa\beta\overline{w'\theta_v'}], \tag{1c}$$

where u, v, and w are the along-wind, cross-wind, and vertical velocity components, θ and θ_v are the potential and virtual potential temperatures, $\kappa = 0.4$ is the von Kármán constant, and $\beta = g/\bar{\theta}_v$ is the buoyancy parameter, where g is gravitational acceleration. Primed terms are deviations from the mean; an overbar indicates an averaging operation.

Nieuwstadt's (1984) theoretical study predicted that locally scaled quantities should approach constant values as the stability parameter, z/L_L, becomes large. Measurements from a meteorological mast were in reasonable agreement with the theory, with scaled quantities becoming constant for values of z/L_L between 1 and 4. Subsequent studies have produced results in broad agreement with Nieuwstadt's, but have tended to encompass a relatively limited range of stabilities and to display a not insignificant degree of scatter between studies (Sorbjan, 1986, 1987; Tjernström and Smedman, 1993; Rogers et al., 1995; Brooks and Rogers, 2000). Shao and Hacker (1990) included a wider range of stabilities in their study and, in contrast to the other studies cited above, found that the scaled velocity variances did not approach constant values as z/L_L became large, but continued to increase in a well-ordered manner. Similar results have been reported by Pahlow et al. (2001)

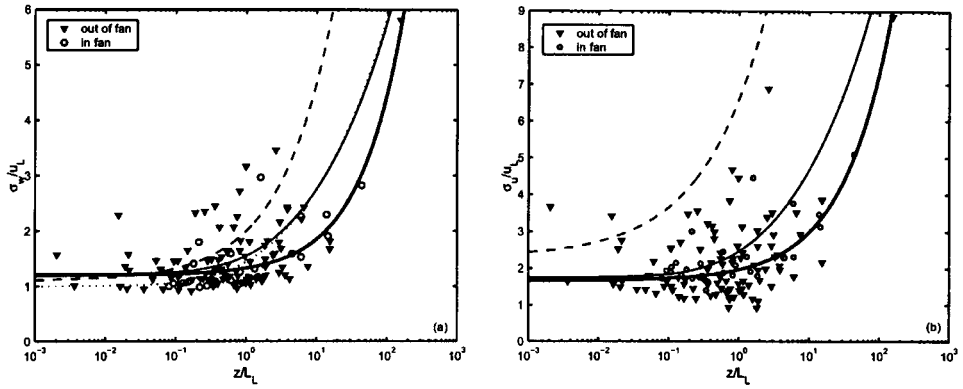

Figure 11. Standard deviations of the vertical (a) and along-stream (b) velocity components normalized by the local velocity scale plotted against the stability parameter z/L_L. The triangles are from locations outside the expansion fan, the circles from locations inside the fan. The thick solid line is a best fit to our entire data set, the dashed line is the empirical function found by Pahlow et al. (2001), the dotted line the function found by Shao and Hacker (1990) (panel (a) only), and the thin solid line the function obtained by Al-Jiboori et al. (2002).

and Al-Jiboori et al. (2002). The former is ostensibly a study of MO similarity under stable conditions, but the scaling parameters were determined at the same level as the variances and fluxes to be scaled and are thus identical with the local scales.

Local scaling quantities have been calculated here for the continuously turbulent IBL from all of the available profiles. Figure 11a shows the scaled standard deviation of vertical velocity plotted against z/L_L. The individual estimates are divided up into those obtained within the expansion fan (triangles) and those from the undisturbed flow outside the fan (circles). Both sets show significant scatter, but there is no systematic difference between them. A curve of the form

$$\frac{\sigma_w}{u_L} = a + b\left(\frac{z}{L_L}\right)^c, \tag{2}$$

has been fitted to the entire data set using a Lorentzian minimization (heavy solid line); this provides a more robust fit than a least squares regression, being less susceptible to bias by outliers. The coefficients for the fitted curve are: $a = 1.2$, $b = 0.13$, $c = 0.7$. Also shown are the curves obtained by Shao and Hacker (1990), Pahlow et al. (2001), and Al-Jiboori et al. (2002). All four data sets show similar behaviour; there are substantial differences between some of the curves at high stabilities, although all lie within the scatter of the present data. The differences in the fitted curves may result in part from biases introduced by the small number of data points at very high stabilities, but the possibility remains that real differences exist in the behaviour of the different flows. Nieuwstadt's (1984) measurements all lie in the range $0.1 < z/L_L < 5$; within this region all three curves lie close to,

and pass through, the value of 1.4 that he found as a constant for σ_w/u_L. Figure 11b shows the scaled standard deviation of the along-stream velocity component, u, for points inside and outside the expansion fan. Again, there is no systematic difference between the two data sets; a curve fitted to the entire data set has coefficients $a = 1.7$, $b = 0.31$, $c = 0.63$. The curve fitted to the scaled cross-stream velocity component, v (not shown), has $a = 1.4$, $b = 0.13$, $c = 0.73$. The horizontal velocity components have greater scatter than the vertical velocity, and the differences between the empirical functions found here and by Pahlow et al. are more substantial; in particular there is a significant difference in the value approached for neutral conditions; the results of Al-Jiboori et al. (2002), however, are much closer to our own.

Figure 12 shows the modelled ABL velocity variances scaled in the same way as the observations in Figure 11; the best fit to the observations is shown as a dashed line for comparison. It is clear that the model reproduces the observed scaling; furthermore, there does not seem to be any systematic difference between the four different areas defined for the model domain; thus the local scaling appears to be a robust feature of this flow. Grant (1992) discusses local scaling from measurements during a near-neutral case over the North Sea during the KONTUR experiment. Among the results shown are variance ratios (σ_V^2/σ_U^2 and σ_W^2/σ_V^2), the stress ratio ($-\langle u'w'\rangle$/TKE) and the momentum flux correlation coefficient ($-\langle u'w'\rangle/\sigma_U\sigma_W$) as a function of normalized boundary-layer height, z/z_i. If local TKE production is balanced by local dissipation, all these ratios should be constant. Grant found that all these profiles change abruptly above $z/z_i \approx 0.5$. While some numerical values differ slightly it is noteworthy that the corresponding profiles modelled here have almost exactly the same functional shape; Figure 13 shows the ratio of wind stress to TKE as an example, with an approximate fit to Grant's data scaled to match the current data in the lower ABL to emphasise the similarity of shape. Grant attributes this deviation to the fact that the turbulence transport term becomes similar in magnitude to the TKE dissipation term in the TKE equation – dissipation and production no longer balance locally. This is also borne out by turbulence measurements in katabatic jets (Horst and Doran, 1988; Smeets et al., 2000). In Grant's near-neutral case this occurred because the dissipation term became small with height while the transport term remained rather small throughout, while in the katabatic cases it was due to an increasing turbulent transport with height.

The ability of the model to simulate the turbulence statistics correctly in the present case, and the fact that the vertical structure of the modelled statistics also conform to the results from Grant (1992), indicate two things. Within the model turbulence scheme variances are prognostic while fluxes derive from analytic expressions; scaling the variances with the local flux will only work if the scaling assumptions underlying this type of turbulence closure scheme are valid. Thus, the close agreement between modelled and observed local scaling functions provides a verification of the validity of the turbulence closure. Secondly, there is an issue of the generality of these results. The model turbulence scheme relies on closure

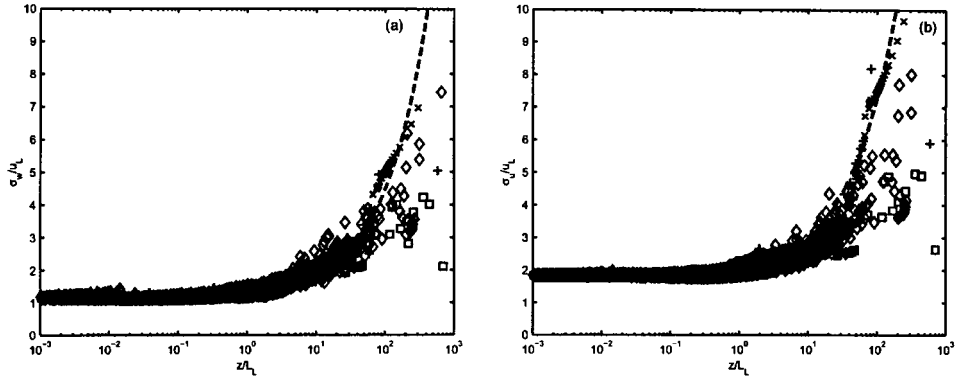

Figure 12. Scaled standard deviations of the vertical velocity (a) and along-stream velocity (b) from the model; the heavy dashed lines are the best fit curves from the observations. The symbols denote the four broad regions of the flow defined in Figure 2b.

constants obtained from independent turbulence measurements both from atmospheric boundary-layer and wind-tunnel studies (Andrén, 1990). The fact that the model turbulence statistics conform to observational local scaling results from two different environments – Grant's (1992) data are from a well-mixed near-neutral ABL with no wind jet, while our data are from an ABL with large static stability and strong low-level wind jet – provides reason to believe both that local similarity is generally applicable where turbulence is continuous, and that the present model can be used to further investigate these relations.

The difference between the empirical scaling function obtained from our aircraft data and the Pahlow et al. (2001) surface-layer data poses the question as to what causes such a substantial difference. Is there a real difference in the scaling between the flows, in which case local scaling cannot be considered universal in its present form, or does the difference arise from measurement biases? The most significant difference between the data sets is that our measurements span the whole turbulent layer, while those of Pahlow et al. were obtained close to the surface.

Figure 14 shows scaled vertical and along-stream velocities partitioned by altitude into three broad groups, z (in m) < 50, $50 \leq z < 200$, and $z \geq 200$. In addition to the profile data used in the analysis so far, we have added data from the four low-level horizontal runs at 30 m in order to provide a small number of additional data points close to the surface. For the vertical velocity all three curves approach a value of about 1.1 for near-neutral conditions, but the curve for the low-level data ($a = 1.1$, $b = 1.8$, $c = 1.2$) rises much faster than that for the high-level ($a = 1.16$, $b = 0.12$, $c = 0.72$) or mid-level ($a = 1.14$, $b = 0.23$, $c = 0.53$) data, which are very similar to each other and to the fit to the entire set of profile derived data (Figure 11a). Similar results are obtained for the along-stream velocity where the high-level ($a = 0.9$, $b = 0.72$, $c = 0.48$) and mid-level ($a = 1.6$, $b = 0.35$, $c = 0.6$) curves are very similar at higher stabilities, while the fit to low-level data ($a = 1.77$,

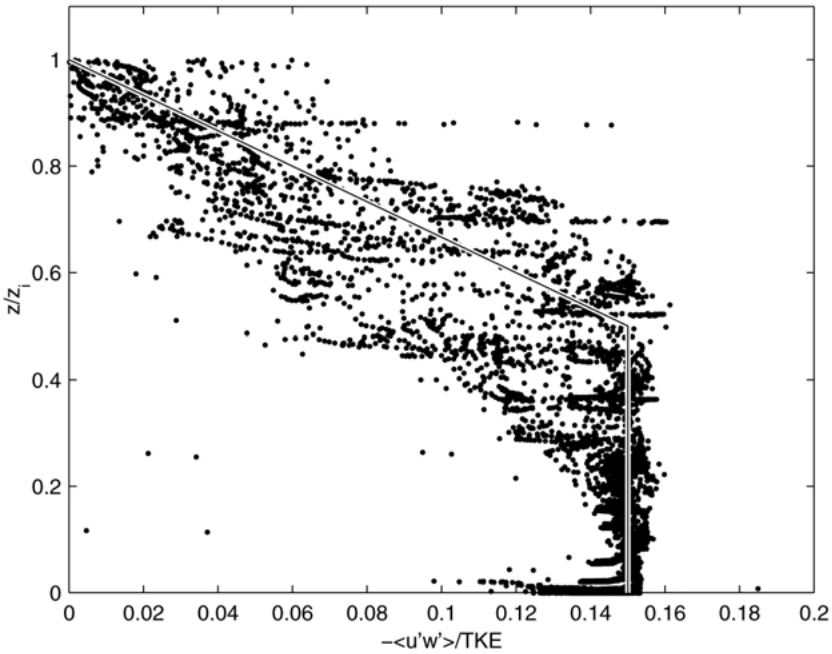

Figure 13. Modelled profiles of the ratio of wind stress to total turbulent kinetic energy. The solid line is an approximate best fit to the results of Grant (1992), scaled to our model results to make the similarity in shape clear.

$b = 2.67$, $c = 1.28$) rises much faster. The curves for low- and mid-level data again approach a similar constant value for near-neutral conditions. The curve for high-level data approaches a rather lower value; this is ascribed to a bias in the curve fit due to the absence of data points for $z/L_L < 0.1$. These results suggest that the apparent differences in scaling behaviour might be related to the proximity to the surface. One possibility is that the apparent change in scaling behaviour is an artefact of the distribution of stability with altitude. The low-level data experience the strongest mixing due to the close proximity of the surface, where shear generation of turbulence is strongest, and hence stratification tends to be only weakly stable – the maximum observed stability is $z/L_L \approx 3$. The very highest stabilities are observed only in the upper part of the turbulent layer. The low-altitude function may thus be biased by the lack of high stability data near the surface. In contrast, data from different height intervals within the model (not shown) occupy different portions of the z/L_L axis but all fall close to the empirical best-fit line. A simple sampling bias between subsets of data does not, however, adequately explain the differences between our results and those of the other studies included in Figure 11. We note also that while several studies have found similarly shaped functions for the scaled velocity variances, none have examined why these functions differ from the constant value predicted by the original local similarity theory.

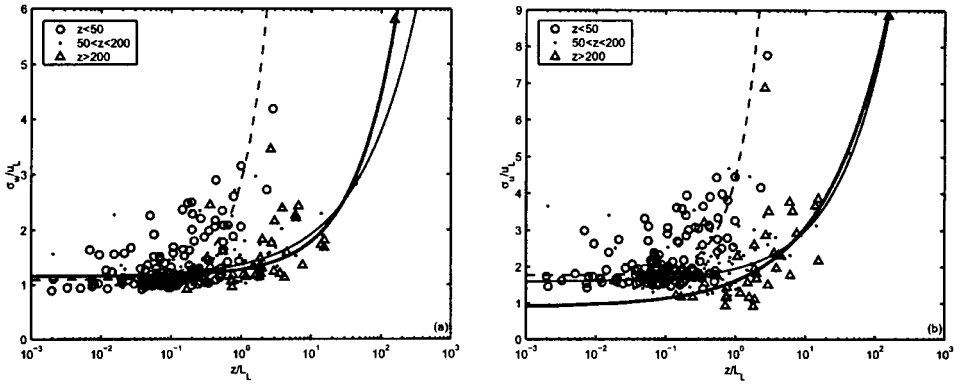

Figure 14. Scaled standard deviations of vertical velocity (a) and along-stream velocity (b) partitioned by altitude: $z < 50$ m – circles and dashed lines; $50 = z < 200$ m – dots and thin solid lines; $z = 200$ m – triangles and heavy solid lines. All data come from within the internal boundary layer.

Nieuwstadt (1984) started with a set of budget equations for velocity and temperature variances, and momentum and temperature fluxes based on second-order closure theory. These were simplified considerably: Coriolis and time-change terms were neglected on the basis that their time scales were much longer than that of turbulence; horizontal advection terms were neglected – an assumption of horizontal homogeneity; and vertical transport terms were neglected because turbulent transport is assumed to be small under stable conditions. At least one of these – the assumption of spatial homogeneity – is clearly invalid for the present study, and for that of Shao and Hacker (1990). We hypothesize that the form of the scaling functions found here is due to the effect of significant stability-dependent non-local transport terms in the variance budgets, and that these curves represent the controlled breakdown of true local similarity. Differences between the scaling functions determined from different studies or sets of data can then be explained by differences in non-local transport between the various flows. Some of the scatter in the observations may also be due to changes in non-local transport at different times or locations within a single data set. In this context we note some subtle trends visible in the results of Pahlow et al. (2001). Their study combined observations from several separate field programs in order to try and avoid biases that might arise due to the specific conditions at a single sight – in effect creating an ensemble average. The scatter observed in their results is comparable with that from other studies; however, close examination of their Figures 1–3 reveals distinct differences between results from the different studies. In particular, in their Figure 2, the data represented by upward pointing triangles lie entirely below their fitted curve for $z/L_L > 0.1$, while most of the data denoted by squares lie above the curve. The distribution of the different data sets with respect to their fitted curves differs for the three velocity components. While these differences could be ascribed to site-specific measurement biases, when considered in the light of results from other

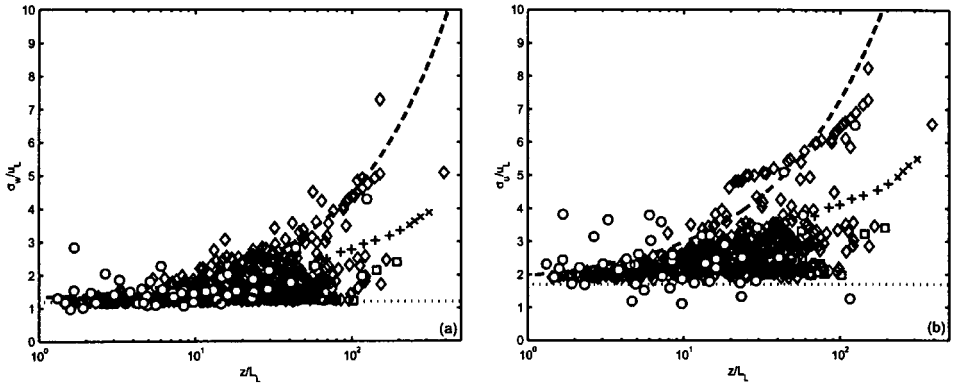

Figure 15. As Figure 12 but for points above the top of the modelled boundary layer. The heavy dashed line is the best fit from the observations and the dotted line is the constant value approached at near-neutral conditions. The circles are observational data obtained in the turbulent region above the expansion fan.

studies, we suggest they may represent true differences in the scaling behaviour. A convincing resolution of this question as to what controls the form of the local similarity scaling functions awaits a more detailed analysis with a more extensive data set.

There are regions above the jet where the static stability is small enough and the wind shear high enough to allow sustained turbulence – this is clear from the model and also indicated by the observations. Turbulence here should not feel the presence of the surface, and exists as a free shear turbulent flow rather than boundary-layer flow. In Figure 15 local scaling is applied to all turbulent model points above the ABL top where $-\overline{w'u'}/u_*^2 > 0.1$. Most of the data points represent the near-coast downstream area above the expansion fan, since this is where the largest area of upward flux persists. The well-defined functional relationship between the scaled quantities and stability appears to break down; it is interesting to note, however, that the normalized variance values are limited on the high side by the best-fit scaling line from the observations and on the lower side by a constant value near the neutral limit of the scaled variance. Also shown are measurements from the turbulent region above the expansion fan (circles); these show more scatter than the model results, but a similar distribution. Pursuing our hypothesis that the observed similarity function is actually dependent upon non-local transport, we can interpret this distribution as being due to a wide degree of variation in non-local transport properties in the volume sampled. The densest concentration of points lies close to the constant defined by neutral conditions, representing conditions where turbulent processes are truly local; other groups of points appear to lie along curves of similar shape to the observational best fit, and may represent regions with similar non-local transport.

5. Conclusions

We have presented the results of a joint observational and modelling study of the mean and turbulence structure of flow around a coastal headland. Key features of the flow are the jet-like structure exhibited by the wind in both the horizontal and vertical, and the formation of an expansion fan in which the flow accelerates and the ABL collapses downstream of Cape Mendocino. Turbulence was generally confined to a stable internal boundary layer except in the region of the expansion fan, where significant turbulence was observed above the collapsed boundary layer – this corresponds to a region of significant upwards momentum flux identified by the numerical simulations above the near-coast side of the wind-speed jet. It is hypothesized that this region becomes turbulent due to a secondary circulation around the wind-speed jet at the inversion bringing warm air from over land out above the jet, reducing the static stability and Richardson number to the point where the wind shear above the jet is able to sustain turbulence.

The model successfully reproduced the major features of the flow, although some discrepancies exist, and the model indicates some structures that cannot be confirmed from the measurements because the observational area is not sufficiently large to encompass them. The wind-speed pattern shows great similarity to the observations, but the upstream winds are too high while the expansion fan wind speed maximum is slightly too low. The upstream wind-stress values are consequently too high; those in the expansion fan are lower than observed, more so than expected from the small wind-speed difference. This is indicative of mixing that is too strong near the surface. The surface fluxes resemble the bulk estimates more than the observed values; this is almost certainly a consequence of the boundary formulation for the modelled turbulence relying on steady-state assumptions. The failure of the model to reproduce the detailed structure of the observed internal boundary layer, and the too rapid cooling of the modelled ABL over the cold pool downstream of the Cape both suggest that mixing may be too efficient within the model; this may be a consequence of the mixing-length formulation, but might also result simply from the limitations imposed by the finite vertical resolution of the model when dealing with very shallow layers.

Local scaling was applied to the standard deviation of the velocity components. Empirical functions fitted to the scaled data follow a similar form to those observed by several previous studies (Shao and Hacker, 1990; Pahlow et al., 2001; Al-Jiboori et al., 2002), though with significant differences in the exact value at high stabilities. The effectiveness of the scaling appeared to remain unaffected by the very significant horizontal variability in mean and turbulence conditions, even through the expansion fan. This is a significant result since it suggests that local scaling is a robust feature of such a flow and can be expected to apply widely. The local scaling was reproduced by the numerical simulations with excellent agreement with the observed scaling function. This provides a strong validation for the turbulence closure scheme utilized within the model, increasing confidence in the reliability of

other turbulence results derived from it. At the same time it indicates a generality in the observational results since the model results depend on a turbulence closure derived from completely independent experimental data. Differences between the empirical scaling functions derived here using data across the whole turbulent layer and by Pahlow et al. (2001), from measurements close to the surface, prompted us to look for a height dependency in the form of the function. Data throughout the larger part of the turbulent layer showed no significant change in scaling behaviour with altitude; however, close to the surface – within the lowest 50 m – the scaling function increases more rapidly with increasing stability than at greater altitude. The present data set is insufficient to determine conclusively the cause of this change in behaviour. A bias in the fitted functions due to the distribution of stability with altitude could explain differences within our own data set, but not those between our results and those of other studies cited here. We also note that the departure of the scaled velocity variances from the constant values predicted by Nieuwstadt's original theory, while being reproduced by several studies, has not been explained. We hypothesize that the form of the observed similarity functions is due to a controlled breakdown of true local scaling under the influence of non-negligible non-local transport terms such as advection, and turbulent and pressure transport terms, in the TKE budget. These non-local processes may differ significantly between different sets of observations, while behaving in a well-defined manner for each case. Thus, the observed local similarity functions appear well-defined for particular sets of observations, but may differ between studies. In order to resolve this question conclusively, a re-assessment of local similarity is required to examine the relationship between the scaling functions and non-local properties of ABL flows.

Acknowledgements

This work was supported by the Office of Naval Research under grant N00014-01-1-0258 (IMB) and N00014-96-1-0002 (MT and SS). The Coastal Waves 96 field program was supported by the National Science Foundation under grant ATM-96-26138.

References

Al-Jiboori, M. H., Xu, Y., and Qian, Y.: 2002, 'Local Similarity Relationships in the Urban Boundary Layer', *Boundary.-Layer Meteorol.* **102**, 63–82.

Andrén, A.: 1990, 'Evaluation of a Turbulence Closure Scheme Suitable for Air-Pollution Applications', *J. Appl. Meteorol.* **29**, 224–239.

Bange, J. and Roth, R.: 1999, 'Helicopter-Borne Flux Measurements in the Nocturnal Boundary Layer over Land – A Case Study', *Boundary-Layer Meteorol.* **92**, 295–325.

Beardsley, R. C., Dorman, C. E., Friehe, C. A., Rosenfeld, L. K., and Winant, C. D.: 1987, 'Local Atmospheric Forcing during the Coastal Ocean Dynamics Experiments. 1. A Description of the Marine Boundary Layer and Atmospheric Conditions over a Northern California Upwelling Region', *J. Geophys. Res.* **92**, 1467–1488.

Brooks, I. M.: 2001, 'Air-Sea Interaction and the Spatial Variability of Surface Evaporation Ducts in a Coastal Environment', *Geophys. Res. Lett.* **28**, 2009–2012.

Brooks, I. M. and Rogers, D. P.: 1997, 'Aircraft Observations of Boundary-Layer Rolls Off the Coast of California', *J. Atmos. Sci.* **54**, 1834–1849.

Brooks, I. M. and Rogers, D. P.: 2000, 'Aircraft Observations of the Mean and Turbulent Structure of a Shallow Boundary Layer over the Persian Gulf', *Boundary-Layer Meteorol.* **95**, 189–210.

Brost, R. A., Lenschow, D. H., and Wyngaard, J. C.: 1982a, 'Marine Stratocumulus Layers. Part I: Mean Conditions', *J. Atmos. Sci.* **39**, 800–817.

Brost, R. A., Wyngaard, J. C., and Lenschow, D. H.: 1982b, 'Marine Stratocumulus Layers. Part II: Turbulence Budgets', *J. Atmos. Sci.* **39**, 818–835.

Burk, S. D. and Thompson, W. T.: 1996, 'The Summertime Low-Level Jet and Marine Boundary Layer Structure along the California Coast', *Mon. Wea. Rev.* **124**, 668–686.

Burk, S. D., Haack, T., and Samelson, R. M.: 1999, 'Mesoscale Simulation of Supercritical, Subcritical, and Transcritical Flow Along Coastal Topography', *J. Atmos. Sci.* **56**, 2780–2795.

Cui, Z., Tjernström, M., and Grisogono, B.: 1998, 'Idealized Simulations of Atmospheric Coastal Flow along the Central Coast of California', *J. Appl. Meteorol.* **37**, 1332–1363.

Dorman, C. E. and Winant, C. D.: 2000, 'The Marine Layer in and around the Santa Barbara Channel', *Mon. Wea. Rev.* **128**, 261–282.

Dorman, C. E., Holt, T., Rogers, D. P., and Edwards, K.: 2000, 'Large-Scale Structure of the June-July 1996 Marine Boundary Layer along California and Oregon', *Mon. Wea. Rev.* **128**, 1632–1652.

Dorman, C. E., Rogers, D. P., Nuss, W., and Thompson, W. T.: 1999, 'Adjustment of the Summer Marine Boundary Layer around Pt. Sur, California', *Mon. Wea. Rev.* **127**, 2143–2159.

Edson, J. B., Beardsley, R. B., McGillis, W. R., Hare, J. E., and Fairall, C. W.: 2000, 'Downward Flux of Moisture over the Ocean', in *Preprint 14th Symposium on Boundary Layers and Turbulence*, American Meteorological Society, 45 Beacon St., Boston, MA, pp. 511–515.

Edwards, K. A.: 2000, 'The Marine Atmospheric Boundary Layer during Coastal Waves 96', Ph.D. Thesis, Scripps Institution of Oceanography, University of California San Diego.

Edwards, K. A., Rogerson, A. M., Winant, C. D., and Rogers, D. P.: 2001, 'Adjustment of the Marine Atmospheric Boundary Layer to a Coastal Cape', *J. Atmos. Sci.* **58**, 1511–1528.

Enger, L.: 1990, 'Simulation of Dispersion in Moderately Complex Terrain – Part A. The Fluid Dynamic Model', *Atmos. Environ.* **24A**, 2431–2446.

Enger, L. and Grisogono, B.: 1998, 'The Response of Bora-Type Flow to Sea-Surface Temperature', *Quart. J. Roy. Meteorol. Soc.* **124**, 1227–1244.

Enger, L., Koracin, D., and Yang, X.: 1993, 'A Numerical Study of the Boundary Layer Dynamics in a Mountain Valley. Part 1: Model Validation and Sensitivity Experiments', *Boundary-Layer Meteorol.* **66**, 357–394.

Enriquez, A. G. and Friehe, C. A.: 1995, 'Effects of Wind Stress and Wind Stress Curl Variability on Coastal Upwelling', *J. Phys. Oceanog.* **25**, 1651–1671.

Grant, A. L. M.: 1992, 'The Structure of Turbulence in the Near-Neutral Atmospheric Boundary Layer', *J. Atmos. Sci.* **49**, 226–239.

Grisogono, B. and Tjernström, M.: 1996, 'Thermal Mesoscale Circulations on the Baltic Coast. 2. Perturbation of Surface Parameters', *J. Geophys. Res.* **101**(D14), 18999–19012.

Haack, T., Burk, S. D., Dorman, C. E., and Rogers, D. P.: 2001, 'Supercritical Flow Interaction between the Cape Blanco – Cape Mendecino Complex', *Mon. Wea. Rev.* **129**, 688–708.

Holt, T. R.: 1996, 'Mesoscale Forcing of a Boundary Layer Jet along the California Coast', *J. Geophys. Res.* **101**, 4235–4254.

Horst, T. W. and Doran, J. C.: 1988, 'The Turbulence Structure of Nocturnal Slope Flow', *J. Atmos. Sci.* **45**, 605–616.

Lenschow, D. H., Zhu, C. J., and Stankov, B. B.: 1988, 'The Stably Stratified Boundary Layer over the Great Plains, I: Mean and Turbulence Structure', *Boundary-Layer Meteorol.* **42**, 95–121.

Mahrt, L.: 1985, 'Vertical Structure in the Very Stable Boundary Layer', *J. Atmos. Sci.* **42**, 2333–2349.

Mellor, G. L. and Yamada, T.: 1982, 'Development of a Closure Model of Geophysical Flows', *Rev. Geophys. Space Phys.* **20**, 851–875.

Nappo, C. J. and Bach, W. D.: 1997, 'Summary Report on the ARO/ARL Workshop on the Stable Planetary Boundary Layer', *Bull. Amer. Meteorol. Soc.* **78**, 493–498.

Nappo, C. J. and Johansson, P.-E.: 1999, 'Summary of the Lövånger International Workshop on Turbulence and Diffusion in the Stable Planetary Boundary Layer', *Boundary-Layer Meteorol.* **90**, 345–374.

Nelson, C. S.: 1977, *Wind Stress Curl over the California Current*, NOAA Tech. Rep. NMFS SSRF-714, 87 pp. [NTIS PB-273-610/6GI].

Nieuwstadt, F. T. M.: 1984, 'The Turbulent Structure of the Stable, Nocturnal Boundary Layer', *J. Atmos. Sci.* **41**, 2202–2216.

Oost, W. A., Jacobs, C. M. J., and Van Oort, C.: 2000, 'Stability Effects on Heat and Moisture Fluxes at Sea', *Boundary-Layer Meteorol.* **95**, 271–302.

Overland, J. E.: 1984, 'Scale Analysis of Marine Winds in Straits and along Mountainous Coasts', *Mon. Wea. Rev.* **112**, 2530–2534.

Pahlow, M., Palange, M. B., and Porté-Agel, F.: 2001, 'On Monin–Obukhov Similarity in the Stable Atmospheric Boundary Layer', *Boundary-Layer Meteorol.* **99**, 225–248.

Pielke, R. A.: 1984, *Mesoscale Meteorological Modelling*, Academic Press, 599 pp.

Rogers, D. P., Dorman, C. E., Edwards, K., Brooks, I. M., Melville, K., Burk, S. D., Thompson, W. T., Holt, T., Ström, L., Tjernström, M., Grisogono, B., Bane, J., Nuss, W., Morley, B., and Schanot, A.: 1998, 'Highlights of Coastal Waves 1996', *Bull. Amer. Meteorol. Soc.* **79**, 1307–1326.

Rogers, D. P., Johnson, D. W., and Friehe, C. A.: 1995, 'The Stable Internal Boundary Layer over a Coastal Sea. I: Airborne Measurements of the Mean and Turbulence Structure', *J. Atmos. Sci.* **52**, 667–683.

Samelson, R. M.: 1992, 'Supercritical Marine-Layer Flow along a Smoothly Varying Coastline', *J. Atmos. Sci.* **49**, 1571–1584.

Shao, Y. and Hacker, J. M.: 1990, 'Local Similarity Relationships in a Horizontally Inhomogeneous Boundary Layer', *Boundary-Layer Meteorol.* **52**, 17–40.

Smeets, C. J. P. P., Duynkerke, P. G., and Vugts, H. F.: 2000, 'Turbulence Characteristics of the Stable Boundary Layer over a Mid-Latitude Glacier, Part II: Pure Katabatic Forcing Conditions', *Boundary-Layer. Meteorol.* **97**, 73–107.

Söderberg, S. and Tjernström, M.: 2001, 'Supercritical Channel Flow in the Coastal Atmospheric Boundary Layer: Idealized Numerical Simulations', *J. Geophys. Res.* **106**(D16), 17811–17829.

Söderberg, S. and Tjernström, M.: 2002, 'Diurnal Cycle of Supercritical Along-Coast Flows', *J. Atmos. Sci.* **59**, 2615–2624.

Sorbjan, Z.: 1986, 'On Similarity in the Atmospheric Boundary Layer', *Boundary-Layer Meteorol.* **34**, 377–397.

Sorbjan, Z.: 1987, 'An Examination of the Local Similarity Theory in the Stably Stratified Boundary Layer', *Boundary-Layer Meteorol.* **38**, 63–71.

Ström, L.: 1999, *Effects of Coastal Forcing on Turbulence and Boundary-Layer Structure*, Ph.D. Thesis, Uppsala University, Sweden.

Sundararajan, R. and Tjernström, M.: 2000, 'Observations and Simulations of a Non-Stationary Coastal Atmospheric Boundary Layer', *Quart. J. Roy. Meteorol. Soc.* **126**, 445–476.

Tjernström, M.: 1993, 'Turbulence Length Scales in Stably Stratified Free Shear Flow Analyzed from Slant Aircraft Profiles', *J. Appl. Meteorol.* **32**, 948–963.

Tjernström, M.: 1999, 'The Sensitivity of Supercritical Atmospheric Boundary-Layer Flow along a Coastal Mountain Barrier', *Tellus* **51A**, 880–901.

Tjernström, M. and Grisogono, B.: 1996, 'Thermal Mesoscale Circulations on the Baltic Coast. 1. A Numerical Case Study', *J. Geophys. Res.* **101**(D14), 18979–18997.

Tjernström, M. and Grisogono, B.: 2000, 'Simulations of Supercritical Flow around Points and Capes in a Coastal Atmosphere', *J. Atmos. Sci.* **57**, 108–135.

Tjernström, M. and Smedman, A.-S.: 1993, 'The Vertical Turbulence Structure of the Coastal Marine Atmospheric Boundary Layer', *J. Geophys. Res.* **98**(C3), 4809–4826.

Yamada, T. and Mellor, G.: 1979, 'A Numerical Simulation of the BOMEX Data Using a Turbulence Closure Model Coupled with Ensemble Cloud Relations', *Quart. J. Roy. Meteorol. Soc.* **105**, 915–944.

Zemba, J. and Friehe, C. A.: 1987, 'The Marine Atmospheric Boundary Layer Jet in the Coastal Ocean Dynamics Experiment', *J. Geophys. Res.* **92**, 1489–1496.